

ARTICLE OPEN



An L-band emitter with quantum memory in silicon

Péter Udvarhelyi^{1,2}, Anton Pershin^{1,2}, Péter Deák¹ and Adam Gali^{1,2}✉

Fluorescent centres in silicon have recently attracted great interest, owing to their remarkable properties for quantum technology. Here, we demonstrate that the C-centre in silicon can realise an optically readable quantum register in the L-band wavelength region where the transmission losses in commercial optical fibres are minimal. Our in-depth theoretical characterisation confirms the assignment of the C-centre to the carbon-oxygen interstitial pair defect. We further explore its magneto-optical properties, such as hyperfine and spin-orbit coupling constants from first principles calculations, which are crucial for tight control of the quantum states of the triplet electron spin. Based on this data, we set up quantum optics protocols to initialise and read out the quantum states of the electron spin, and realise a quantum memory by transferring quantum information from the electron spin to proximate ²⁹Si nuclear spins. Our findings establish an optically readable long-living quantum memory in silicon where the scalability of qubits may be achieved by CMOS-compatible technology.

npj Computational Materials (2022)8:262; <https://doi.org/10.1038/s41524-022-00957-7>

INTRODUCTION

Silicon is a mature platform for quantum technology, offering multiple advantages for the integration of defect quantum emitters. As compared to other host materials¹, high-purity isotopically enriched single crystals of silicon^{2,3} and integrated photonic devices^{4,5} are readily available. These characteristics of the host material enable the improvement of optical and spin properties of the quantum defects. Recent experimental advances allowed for the isolation of single quantum emitters in this material, such as G-, W- and T-centres, with a great promise for quantum communication^{6–17}. However, to further reduce the transmission losses in optical fibres, it is essential to find an active defect with the emission wavelength in either the L- or the C-band and an optically addressable spin state. This caused a revival of interest in the magneto-optical properties of deep defects in silicon, including those configurations that have been discovered decades ago^{11,18–21}.

Carbon and oxygen atoms are the most common impurities and therefore are important sources of colour centres in silicon crystals. When both are present in a sample, the oxygen interstitial is able to trap a mobile carbon atom, forming a carbon–oxygen interstitial pair (C_iO_i)^{22,23}. This stable defect complex was thoroughly characterised by various experimental techniques. Its photoluminescence (PL) signal was associated with the C-line at 789 meV^{24,25} in the spin singlet, neutral charge state²⁶ and with the Si-G15 electron paramagnetic resonance (EPR) centre in the spin doublet, positive charge state²⁷. Local vibrational modes (LVM) in the PL spectrum were identified at 64.5, 72.6, 138.1, and 145.3 meV energies^{24,25}. The uniaxial stress perturbation effect on the PL line was consistent with C_{1h} point symmetry²⁶. Deep-level transient spectroscopy (DLTS) measurements identify a deep donor level at $E_{\text{VBM}} + 360$ meV position²⁸. Time-resolved PL measurements reveal the excited state lifetime of 2.3 μs at cryogenic temperatures and a second slower decay activated at elevated temperatures with an activation energy of 3.1 meV²⁹. The latter was associated with a reverse intersystem crossing (rISC) from a lower-lying triplet excited state. From the measurements, radiative and ISC lifetimes of 14 and 2.8 μs were obtained,

respectively. PL excitation measurements reported a series of excited states, revealing the bound exciton origin of the C-line³⁰. It was assumed, that the triplet state is dark owing to the quenched orbital momentum of the hole by the defect strain field. However, this phosphorescence was detected at low temperatures despite the measured isotropic *g*-factor in the triplet state³¹.

The defect structure was tentatively identified^{32,33} using density functional theory (DFT) calculation within the local density approximation (LDA)^{34,35}. The identification was based on the calculated LVMs and the position of the donor level, where the latter could be compromised by the underestimation of the band gap by DFT-LDA method. The atomic structure of the defect is shown in Fig. 1a. It represents a pair of neighbouring Si–C and Si–O defects, connected into a square-like structure by a mutual displacement from the initial split-interstitial positions towards the opposite directions (up–down configuration)³⁶.

The C-centre in silicon exhibits emission in the telecom L-band with a confirmed high electron spin state which has a great potential in quantum communication with the possibility of scalable creation of the quantum emitters in carbon and oxygen-contaminated silicon by CMOS compatible technology (e.g., ref. 12). However, the lack of understanding the nature of the electronic structure and the origin of the emission of the C-centre precludes it from being considered as a qubit. In this work, we aim to significantly advance the magneto-optical characterisation of the C_iO_i⁰ defect by means of high-level DFT calculations, in order to elaborate on the feasible quantum optics protocols for quantum technology applications. To this end, we determine the key zero-field splitting (ZFS) parameters of the defect, taking into account the effects of hyperfine and spin–orbit-interaction. We propose a spin-selective optical cycle for the coherent manipulation and sensitive readout of the triplet electron spin state, suitable for the optically detected magnetic resonance (ODMR) measurements. Hyperfine interaction between the electron and proximate nuclear spins mediates to realise a quantum register with long-living memory as the ground state singlet does not disturb the proximate nuclear spin states.

¹Wigner Research Centre for Physics, P.O. Box 49, H-1525 Budapest, Hungary. ²Budapest University of Technology and Economics, Institute of Physics, Department of Atomic Physics, Műegyetem rakpart 3., 1111 Budapest, Hungary. ✉email: gali.adam@wigner.hu

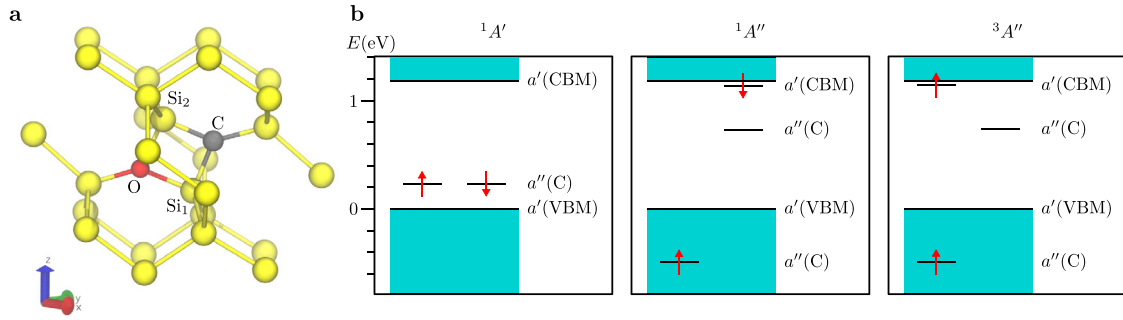


Fig. 1 Geometry and electronic structure of the defect. **a** The atomic structure of the C_iO_i defect complex, consisting of neighbouring carbon (C_i-Si_1) and oxygen (O_i-Si_2) split-interstitial defects. **b** Kohn-Sham level structure of the $C_iO_i^0$ defect ground state ($^1A'$), singlet ($^1A''$), and triplet ($^3A''$) excited states in the spin-polarised HSE06 calculation. VBM, CBM, and C labels show the valence band maximum, the conduction band minimum and the dangling bond orbital of the carbon atom, respectively.

RESULTS

Electronic structure

The calculated electronic structure of the $C_iO_i^0$ defect is shown in Fig. 1b. The only in-gap state is induced by the carbon impurity dangling bond resulting in a deep donor level. The calculated (+/0) charge transition level of $E_{VBM} + 408$ meV is in good agreement with the DLTS level (360 meV)²⁸. Note that we label the states by their irreducible representations in the C_{1h} point symmetry group. The $^1A'$ is the ground state with two electrons occupying the deep defect level. Promoting one electron from the deep level to the conduction band minimum in the same or opposite spin channel results in the singlet and triplet excited states, respectively. In the double group notation, the irreducible representations of these semi-localised defect states, formulated in the two-electron representation in the orbital and spin product basis, are as follows

$$|^1A'\rangle = \frac{1}{\sqrt{2}} |a''a''\rangle \otimes |\uparrow\downarrow - \downarrow\uparrow\rangle = |\Gamma_1\rangle, \quad (1)$$

$$|^1A''\rangle = \frac{1}{2} |a''a' + a'a''\rangle \otimes |\uparrow\downarrow - \downarrow\uparrow\rangle = |\Gamma_2\rangle, \quad (2)$$

$$|^3A''\rangle = \frac{1}{2} |a''a' - a'a''\rangle \otimes |\uparrow\downarrow + \downarrow\uparrow\rangle = |\Gamma_2\rangle, \quad (3)$$

$$|^3_{\pm}A''\rangle = \frac{1}{2} |a''a' - a'a''\rangle \otimes |\uparrow\uparrow \pm \downarrow\downarrow\rangle = |\Gamma_1\rangle. \quad (4)$$

The calculated zero-phonon line (ZPL) energy in the singlet-singlet transition is 750 meV after the same finite size correction as for the charge transition level calculation was applied (see Methods). This correction is justified by the excitonic nature of the excited states, where the electrostatic potential of the localised hole is corrected similarly to the ionised ground state³⁷. The calculated ZPL energy is smaller than the calculated donor transition energy ($E_{CBM} - E_{(+/0)} = 780$ meV), leading to a stable neutral emitter. We obtain the energy of the triplet level to be 2.8 meV below the singlet excited state, in good agreement with the temperature activation energy (3.1 meV) for the rISC process²⁹. We validate our HSE06 DFT results by comparison with GOWO and Bethe-Salpeter-equation (GOWO+BSE) calculations in 216-atom supercell model^{38–40} (see Supplementary Note 3). To this end, we use the HSE06 relaxed ground state atomic positions as the computation of the quantum mechanical forces at the GOWO+BSE level has not yet been implemented. Thus, we can compare the ground state electronic structure and the vertical excitation energies in both calculation methods. We obtain energy differences between the HSE06 Δ SCF and GOWO+BSE calculations of 11 and 15 meV for the vertical excitation energy and the excited state singlet-triplet splitting, respectively. The GOWO+BSE exciton wavefunction is dominated by a single Slater

determinant in complete agreement with the Δ SCF electronic configuration. This justifies the Δ SCF method for the excitation calculations of the defect.

Spin properties

After obtaining the electronic states, we explore the spin interactions crucial for the tight control of the quantum bit defect. We start with the calculation of the dipolar spin-spin interaction of the electron spin in the triplet excited state, governed by the Hamiltonian operator

$$\hat{H}_{SS} = D \left(\hat{S}_z^2 - \frac{S(S+1)}{3} \right) + \frac{E}{2} (\hat{S}_+^2 + \hat{S}_-^2). \quad (5)$$

Our calculations result in axial $D = -771$ MHz and rhombic $E = 94$ MHz ZFS parameters. In order to describe the new eigenstates, we introduce the magnetic quantum number m_S in the notation. The D parameter lifts the degeneracy of the triplet state to $2\Gamma_1(\pm) + \Gamma_2(0)$, while E further splits the ± 1 spin states resulting in $\Gamma_1(-)$, $\Gamma_1(+)$, $\Gamma_2(0)$, in ascending energy order.

Spin-orbit coupling is described by the Hamiltonian operator

$$\hat{H}_{SO} = \lambda_z \hat{L}_z \hat{S}_z + \lambda_+ \hat{L}_+ \hat{S}_- + \lambda_- \hat{L}_- \hat{S}_+, \quad (6)$$

which belongs to the totally symmetric Γ_1 irreducible representation in the double group. The selection rules for spin-orbit coupling are depicted in Fig. 3a. We further express the two-particle operators in (6) with single-particle ones ($\hat{I}_z \hat{S}_z$, $\hat{I}_{\pm} \hat{S}_{\pm}$) and expand the matrix elements between one-particle spin-orbitals (see Supplementary Note 1). Furthermore, we substitute the DFT-calculated matrix elements Λ_{ij} of the spin-orbit Hamiltonian expanded on the ordered basis functions of the one-particle spin-orbitals in the above expansion, namely,

$$\Lambda[\text{meV}] = \begin{pmatrix} |a''\uparrow\rangle & |a''\downarrow\rangle & |a'\uparrow\rangle & |a'\downarrow\rangle \\ \begin{pmatrix} 0.186 & 0 & 0 & 0.082 + 0.061i \\ & 0.735 & 0.235 & 0 \\ & & -0.010 & 0 \\ & & & -0.010 \end{pmatrix} \end{pmatrix} \quad (7)$$

This way, the spin-orbit couplings to each sublevel are obtained as follows

$$\lambda_z = \frac{1}{2} (\Lambda_{11} - \Lambda_{22} - \Lambda_{33} + \Lambda_{44}) = -0.275 \text{ meV}, \quad (8)$$

$$\lambda_- = \frac{1}{\sqrt{2}} (\Lambda_{23} + \Lambda_{14}) = (0.223 + 0.043i) \text{ meV}, \quad (9)$$

$$\lambda_+ = \frac{1}{\sqrt{2}} (\Lambda_{23} - \Lambda_{14}) = (0.108 - 0.043i) \text{ meV}. \quad (10)$$

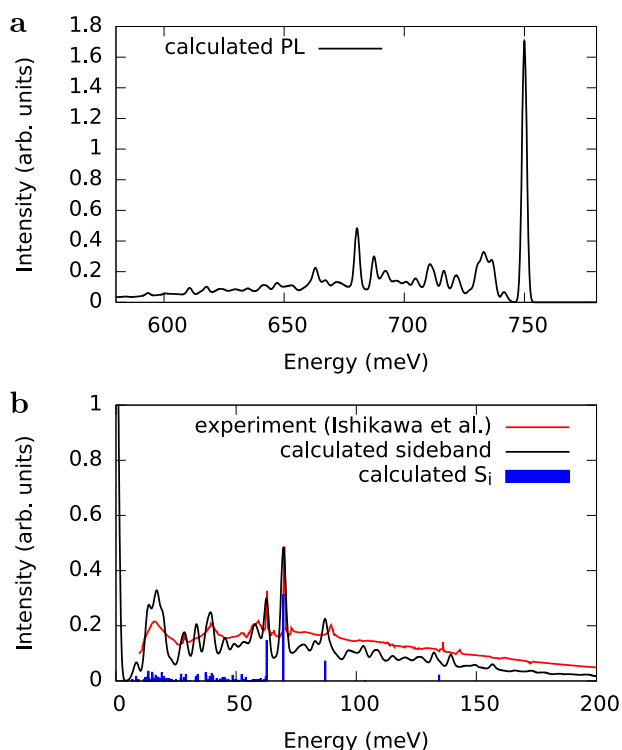


Fig. 2 Simulated photoluminescence spectrum. **a** Calculated PL spectrum of $C_iO_i^0$ defect, showing Huang-Rhys factor of $S = 2.1$. **b** Calculated PL sideband relative to the ZPL energy and the S_i partial Huang-Rhys factors. Our results are compared to the experimental PL sideband reported by Ishikawa et al.³¹.

The spin-orbit coupling of the singlet and triplet states reshapes the relative energies of the spin sublevels within the excited triplet state. It provides a large stabilisation for the $m_S = 0$ level, but is negligible for the other two sublevels, owing to the differences in the energy gaps. Thus, the axial ZFS parameter is modified to $D = 5.7$ GHz, which is in reasonable agreement with the ~ 3 GHz readout from the broad peaks in the magneto-PL spectrum³¹. The re-normalisation also leads to a strong mixing of the excited state singlet and triplet $m_S = 0$ levels, manifesting as a 1% contribution of the triplet state to the excited singlet state.

In addition, we calculate the hyperfine interaction

$$\hat{H}_{hyp} = A_{xx}\hat{I}_x\hat{S}_x + A_{yy}\hat{I}_y\hat{S}_y + A_{zz}\hat{I}_z\hat{S}_z \quad (11)$$

at ^{13}C , ^{17}O , and ^{29}Si isotopes surrounding the defect (see Supplementary Note 2). We conclude that the hyperfine interaction in the neutral triplet excited state of the defect is very similar to that of the positive doublet ground state, only incorporating a scaling factor of 2 of the two spin quantum numbers in the neutral and positive charge states. It can be explained by the delocalised nature of the excitonic excited state, so the similar hole spin density governs the interaction as for the positively charged defect. We find good agreement for the calculated positively charged defect ^{13}C hyperfine parameters of $A_{xx} = 5.9$ MHz, $A_{yy} = 5.2$ MHz and $A_{zz} = 153.9$ MHz with the reported values of the Si-G15 EPR centre²⁷. The corresponding values in the neutral triplet state are $A_{xx} = 3.1$ MHz, $A_{yy} = 2.7$ MHz and $A_{zz} = 77.2$ MHz. Additionally, we report the hyperfine couplings of nearest-neighbour (NN) and next-NN (NNN) silicon nuclei [see Supplementary Table 1 and Supplementary Fig. 1a].

Optical properties

Having characterised the spin properties of the defect, we turn to the detailed description of the optical transitions. First, we

calculate the phonon spectrum and simulate the PL spectrum [see Fig. 2a] according to the Franck-Condon principle. We obtain a sideband with LVMs at 63, 70 and 134 meV energies closely resembling the experimental spectrum^{24,25,31}. We also observe an LVM at 87 meV, giving rise to a respective weak experimental signal [see Fig. 2b]. The calculated Huang-Rhys factor is 2.1, corresponding to a Debye-Waller factor of 12%. The bound exciton nature of the excitation results in a relatively delocalised electron orbital, accounting for the observed long optical lifetime in experiments²⁹.

Owing to the spin-orbit coupling, ISC and phosphorescence processes can also connect the singlet ground and excited states in a spin-selective optical cycle. The strong mixing with λ_z spin-orbit coupling in the excited state enables a triplet signal with considerable intensity. According to our spin-orbit calculations, the intensity ratio of the triplet phosphorescence is 1% for the $m_S = 0$ state in the triplet manifold, in good agreement with the experimental findings³¹. This results in about 1.4 ms radiative lifetime for this state. On the other hand, allowing the intersystem crossing to the ground state can be formulated as a first-order perturbation for the $m_S = -1$ and $m_S = +1$ branches of the triplet (see Methods). Our calculations yield weak transition dipoles of 0.004D and 0.002D for the $m_S = -1$ and $m_S = +1$ phosphorescence branches, respectively, which have very long (>10 ms) radiative lifetimes.

The optical properties of the C-centre can be compared to other promising quantum defects in silicon. The G- and T-centres emit in the telecommunication O-band^{9,16,17} and the W-centre emits near the short wavelength edge of this band¹¹. The emission of the Er^{+3} ion lies in the C-band⁴¹, whereas the C-centre exhibits ZPL in the most favourable L-band^{24,25}, regarding the optical fibre transmission loss. However, the former shows a very long radiative lifetime of about 1–2 ms^{42,43}, which can be decreased 10-fold with integration inside silicon waveguides⁴⁴. Moreover, emission enhancement up to 70-fold was demonstrated by embedding erbium ions in a Fabry-Perot resonator⁴⁵. The radiative lifetime of ensemble G-centres was reported to be 5.9 ns⁴⁶, and a ~ 40 times enhancement in the PL intensity was achieved by resonant coupling to a dielectric meta-surface⁴⁷. The emission of the excitonic excited states is much dimmer, as reported for the T-centre with 940 ns excited state lifetime¹⁶; however, Purcell enhancement was demonstrated for up to ~ 58 -fold increase in the emission intensity¹⁷. Since the nature of the C-centre optical excitation is reminiscent of that of the W- and T-centres, we can assume that the integration in optical resonators could lead to a large Purcell-enhancement, as was already demonstrated for the G- and T-centres, making the relatively dim PL and phosphorescence of the C-centre significantly brighter.

Quantum protocols

We propose a quantum optical protocol to utilise the metastable triplet state and its phosphorescence for ODMR and its hyperfine coupling to nearby nuclear spins for quantum register applications. Optical initialisation of the triplet spin state is feasible owing to this spin-selective ISC to $m_S = 0$ state. The $m_S = \pm 1$ states are dark in the phosphorescence, suggested by their calculated very long lifetime. We predict an ODMR contrast detected in the phosphorescence signal, where the spin rotation between the bright $|0\rangle$ and the dark $|\pm 1\rangle$ states decrease the phosphorescence intensity [see Fig. 3a]. The ODMR contrast diminishes at elevated temperatures together with the phosphorescence signal itself, owing to the activated rISC rate.

A long-lived quantum memory can be achieved in the defect by transferring the coherent electron spin state to the nuclear spin manifold. This can be achieved by Landau-Zener transitions^{48,49} at

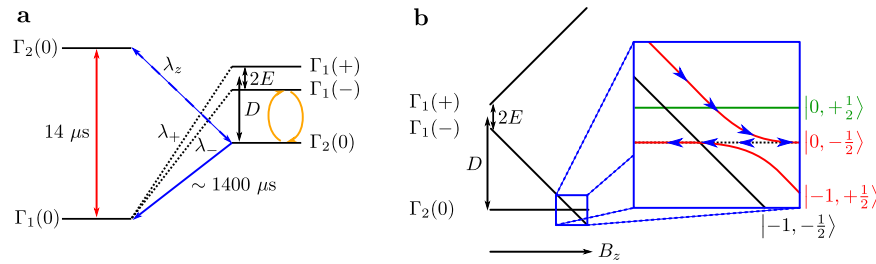


Fig. 3 Proposed quantum protocols. **a** Quantum protocol for ODMR in C-centre. The red and blue arrows show fluorescence and phosphorescence, respectively. The blue dashed arrow highlights the spin-selective ISC leading to the main contribution to phosphorescence. The dotted lines represent the weak ISC to the ground state. Orange lines correspond to coherent spin control using microwave excitation. The spin–spin interaction incorporates both dipolar spin coupling and the re-normalisation effect from the spin-orbit interaction. The spin-selective ISC initialises the bright $|0\rangle$ spin state. Applying spin rotation leads to a contrast in the phosphorescence emission. **b** Magnetic field dependence of the triplet electronic and doublet nuclear spin levels labelled by $|m_s, m_l\rangle$. Procedure for the Landau-Zener transition is highlighted for negative hyperfine coupling parameters. The initial superposition (green and red) of electronic states $\alpha|0, +\frac{1}{2}\rangle + \beta|-1, +\frac{1}{2}\rangle$ is transferred to the coherent superposition of nuclear states $\alpha|0, +\frac{1}{2}\rangle + \beta|0, -\frac{1}{2}\rangle$. The degenerate $|0, \pm\frac{1}{2}\rangle$ hyperfine levels are separated for the sake of clarity.

the triplet state level anti-crossing (LAC) condition

$$\alpha\left|0, +\frac{1}{2}\right\rangle + \beta\left|-1, +\frac{1}{2}\right\rangle \xrightarrow{\text{LZ}} \alpha\left|0, +\frac{1}{2}\right\rangle + \beta\left|0, -\frac{1}{2}\right\rangle, \quad (12)$$

where we note the electron and nuclear spin magnetic levels as $|m_s, m_l\rangle$. The nuclear spin flip-flop process is feasible utilising the perpendicular hyperfine couplings (A_{xx}, A_{yy}) to nearby nuclei. We calculate such couplings to be larger than 10 MHz for several positions of the ^{29}Si nuclei (see Supplementary Table 1), allowing for short ramp time of the magnetic field sweep across the LAC [see Fig. 3b], however, decreasing the electron spin coherence time. As a compromise between operation speed and decoherence due to the hyperfine interaction itself, we suggest further lying atoms with hyperfine couplings in the order of 1 MHz as the quantum registers [see Supplementary Fig. 1b]. Alternatively, a weak magnetic field perpendicular to the nuclear spin quantisation axis (set by A_{zz}) and a resonant microwave excitation pulse can also be utilised to map the electron spin superposition onto the nuclear spin as demonstrated for NV centre and a single ^{13}C in diamond in ref. ⁵⁰. The former allows for Larmor precession in the degenerate nuclear spin manifold of the $m_s = 0$ state, while the latter is tuned to the hyperfine resonance at $D - E - \frac{A_{zz}}{2}$ energy.

$$\alpha\left|0, +\frac{1}{2}\right\rangle + \beta\left|-1, +\frac{1}{2}\right\rangle \xrightarrow{\pi} \alpha\left|0, -\frac{1}{2}\right\rangle + \beta\left|-1, +\frac{1}{2}\right\rangle \xrightarrow{\pi_{\text{MW}}} \alpha\left|0, -\frac{1}{2}\right\rangle + \beta\left|0, +\frac{1}{2}\right\rangle. \quad (13)$$

where π_L and π_{MW} are π pulses in the nuclear and electron spin manifolds, respectively. The readout of the nuclear spin memory into the electron spin manifold utilises the same magnetic field sweep as the storage process, however, it is the inverse process for the above pulse sequence. The initialisation of the nuclear spin is feasible with subsequent memory readout and optical pumping processes. We note that there are methods for the fast manipulation of multi-qubit registers with a combination of microwave and radio frequency pulses as well^{51,52}. Based on the above initialisation, storage, and readout protocols, the individual control of the electron spin of the C-centre and a nearby single nuclear spin is feasible for the realisation of long-living quantum memory. Additionally, as the excited triplet state relaxes to the singlet ground state of the defect, further decoherence by the hyperfine coupling to the electron spin is eliminated, increasing the coherence time of the nuclear spin register. We note that isotope engineering of silicon is viable to find the optimum operation conditions, similar to the recent results for divacancy qubits in silicon carbide⁵³.

There are quantum memories already investigated in silicon, the spin doublet T-centre⁵⁴ and the Er^{+3} ion⁴¹, showing favourable spin coherence properties. For the former one, ODMR was

demonstrated using spin selective resonant optical excitation (hyperpolarization method) reporting $T_1 > 16$ s and Hahn-echo T_2 times exceeding a millisecond and a second for the electron and hydrogen nuclear spins, respectively¹⁶. The erbium ion shows shorter coherence times of $T_1 \sim 1$ ms and $T_2 = 7.5 \mu\text{s}$ ⁵⁵. However, the advantage of the singlet ground state for the increased nuclear spin coherence was proposed for the ST1 and TR12 centres in diamond as well^{56,57}. These successful applications call for the need for an in-depth experimental study on the spin dynamics in the C-centre as well for a direct comparison to the above contenders.

DISCUSSION

The C_iO_i^0 defect in silicon, identified as the C-centre, was investigated for quantum technology applications. We obtain electronic structures in-line with experimental observations. We explore the spin interactions in the defect and report rhombic ZFS values crucial for the coherent manipulation of the electron spin qubit. We determine the symmetry-allowed spin–orbit couplings, revealing ISC transition with λ_z coupling between the excited states, and with different λ_{\pm} coupling strength from the $m_s = \pm 1$ substates of the triplet excited state is coupled to the ground state. These phosphorescence transitions correspond to the observed triplet radiative transition at cryogenic temperatures³¹. The lack of phosphorescence at elevated temperatures can be explained by a thermally activated rISC process, thermalising the excited states. On the other hand, population trapping in the triplet state is feasible at cryogenic temperatures, increasing the relative intensity of the phosphorescence assisted by the spin–orbit mixing with the close-lying excited singlet state. We conclude that C-centre in silicon is not only a promising single photon source for quantum communication applications via telecommunication optical fibres, but optical readout of the spin state is feasible in its triplet excited state. This opens the door for several quantum technology applications utilising this defect, including cryogenic temperature nanoscale sensing and quantum communication applications.

METHODS

Details on DFT calculations

The atomic structure of the defect is modelled in a 512-atom silicon supercell. To this end, we used the Heyd–Scuseria–Ernzerhof (HSE06) functional⁵⁸ and Γ -point sampling of the Brillouin zone, as implemented in the VASP plane wave-based code^{59–62}. For the description of core electrons, projector augmented wave pseudo-potentials are used^{63,64}.

Excited states were calculated with the Δ SCF method⁶⁵. The finite size correction of the charged supercells is obtained from self-consistent potential correction method⁶⁶ to be 56 meV. The spin–spin contribution to the ZFS parameters was calculated by the approach of Bodrog and Gali⁶⁷ using the VASP implementation of Martijn Marsman. The Perdew–Burke–Ernzerhof⁶⁸ functional was employed to compute the phonon spectrum as well as in the non-collinear DFT calculations in order to manage the computational cost.

Details on GW calculations

GW0³⁸ and BSE^{39,40} calculations were performed using VASP in a 216-atom supercell model, keeping the Γ -point sampling. The orbital basis was calculated with DFT HSE06 functional, with a number of unoccupied orbitals more than 10 times the occupied ones. The energy cutoff for the calculation of the response function was limited to 150 eV to manage the computational workload. BSE was calculated beyond the Tamm–Dancoff approximation⁶⁹, including 100 occupied and 100 unoccupied orbitals.

Calculation of phosphorescence rates

The transition dipole of the phosphorescence process between the triplet excited and singlet ground state can be calculated from perturbation theory as⁷⁰

$$\langle {}^1A' | \mathbf{er} | {}^3A'' \rangle = \Delta\mu \frac{\langle {}^1A' | \hat{\lambda} \hat{L} \hat{S} | {}^3A'' \rangle}{E({}^1A') - E({}^3A'')} \quad (14)$$

where $\Delta\mu = \langle {}^3A'' | \mathbf{er} | {}^3A'' \rangle - \langle {}^1A' | \mathbf{er} | {}^1A' \rangle = 13.7$ D is the change of the macroscopic dipole moment in the transition.

DATA AVAILABILITY

The authors declare that the main data supporting the findings of this study are available within the paper and its Supplementary files. Part of the source data is provided in this paper. The data that support the findings of this study are available from the corresponding author upon reasonable request.

CODE AVAILABILITY

The codes that were used in this study are available upon request to the corresponding author.

Received: 5 July 2022; Accepted: 14 December 2022;

Published online: 29 December 2022

REFERENCES

- Zhang, G., Cheng, Y., Chou, J.-P. & Gali, A. Material platforms for defect qubits and single-photon emitters. *Appl. Phys. Rev.* **7**, 031308 (2020).
- Itoh, K. M. et al. High purity isotopically enriched ²⁹Si and ³⁰Si single crystals: Isotope separation, purification, and growth. *Jpn. J. Appl. Phys.* **42**, 6248–6251 (2003).
- Chartrand, C. et al. Highly enriched ²⁸Si reveals remarkable optical linewidths and fine structure for well-known damage centers. *Phys. Rev. B* **98**, 195201 (2018).
- Wong, H., Filip, V., Wong, C. & Chung, P. Silicon integrated photonics begins to revolutionize. *Microelectron. Reliab.* **47**, 1–10 (2007).
- Hollenbach, M. et al. A photonic platform hosting telecom photon emitters in silicon. Preprint at *arXiv* <https://arxiv.org/abs/2112.02680> (2021).
- Buckley, S. et al. All-silicon light-emitting diodes waveguide-integrated with superconducting single-photon detectors. *Appl. Phys. Lett.* **111**, 141101 (2017).
- Buckley, S. M. et al. Optimization of photoluminescence from w centers in silicon-insulator. *Opt. Express* **28**, 16057–16072 (2020).
- Hollenbach, M., Berencén, Y., Kentsch, U., Helm, M. & Astakhov, G. V. Engineering telecom single-photon emitters in silicon for scalable quantum photonics. *Opt. Express* **28**, 26111–26121 (2020).
- Redjem, W. et al. Single artificial atoms in silicon emitting at telecom wavelengths. *Nat. Electron.* **3**, 738–743 (2020).

- Tait, A. N. et al. Microring resonator-coupled photoluminescence from silicon w centers. *J. Phys. Photonics* **2**, 045001 (2020).
- Baron, Y. et al. Detection of single w-centers in silicon. *ACS Photonics* **9**, 2337–2345 (2022).
- Hollenbach, M. et al. Wafer-scale nanofabrication of telecom single-photon emitters in silicon. <https://www.nature.com/articles/s41467-022-35051-5> (2022).
- Baron, Y. et al. Single g centers in silicon fabricated by co-implantation with carbon and proton. *Appl. Phys. Lett.* **121**, 084003 (2022).
- Redjem, W. et al. Defect engineering of silicon with ion pulses from laser acceleration. Preprint at *arXiv* <https://arxiv.org/abs/2203.13781> (2022).
- Prabhu, M. et al. Individually addressable artificial atoms in silicon photonics. Preprint at *arXiv* <https://arxiv.org/abs/2202.02342> (2022).
- Bergeron, L. et al. Silicon-integrated telecommunications photon-spin interface. *PRX Quantum* **1**, 020301 (2020).
- Higginbottom, D. B. et al. Optical observation of single spins in silicon. *Nature* **607**, 266–270 (2022).
- Durand, A. et al. Broad diversity of near-infrared single-photon emitters in silicon. *Phys. Rev. Lett.* **126**, 083602 (2021).
- Udvarhelyi, P., Somogyi, B., Thiering, Gm. H. & Gali, A. Identification of a telecom wavelength single photon emitter in silicon. *Phys. Rev. Lett.* **127**, 196402 (2021).
- Chen, M., Baer, R., Neuhauser, D. & Rabani, E. Stochastic density functional theory: Real- and energy-space fragmentation for noise reduction. *J. Chem. Phys.* **154**, 204108 (2021).
- Dhaliah, D., Xiong, Y., Sipahigil, A., Griffin, S. M. & Hautier, G. First principles study of the t-center in silicon. <https://journals.aps.org/prmaterials/abstract/10.1103/PhysRevMaterials.6.L053201>.
- Davies, G. Carbon-related processes in crystalline silicon. In *Defects in Semiconductors 15*, vol. 38 of *Materials Science Forum*, 151–158 (Trans Tech Publications Ltd., 1989).
- Ayedh, H. M., Monakhov, E. V. & Coutinho, J. Formation and dissociation reactions of complexes involving interstitial carbon and oxygen defects in silicon. *Phys. Rev. Mater.* **4**, 064601 (2020).
- Thonke, K., Watkins, G. & Sauer, R. Carbon and oxygen isotope effects in the 0.79 eV defect photoluminescence spectrum in irradiated silicon. *Solid State Commun.* **51**, 127–130 (1984).
- Davies, G., Lightowlers, E. C., Newman, R. C. & Oates, A. S. A model for radiation damage effects in carbon-doped crystalline silicon. *Semicond. Sci. Technol.* **2**, 524–532 (1987).
- Thonke, K., Hangleiter, A., Wagner, J. & Sauer, R. 0.79 eV (c line) defect in irradiated oxygen-rich silicon: excited state structure, internal strain and luminescence decay time. *J. Phys. C Solid State Phys.* **18**, L795–L801 (1985).
- Trombetta, J. M. & Watkins, G. D. Identification of an interstitial carbon—interstitial oxygen complex in silicon. *MRS Proc.* **104**, 93 (1987).
- Ayedh, H. M., Grigorev, A. A., Galeckas, A., Svensson, B. G. & Monakhov, E. V. Annealing kinetics of the interstitial carbon-dioxygen complex in silicon. *Phys. Status Solidi A* **216**, 1800986 (2019).
- Bohnert, G., Weronnek, K. & Hangleiter, A. Transient characteristics of isoelectronic bound excitons at hole-attractive defects in silicon: The c(0.79 eV), p(0.767 eV), and h(0.926 eV) lines. *Phys. Rev. B* **48**, 14973–14981 (1993).
- Wagner, J., Thonke, K. & Sauer, R. Excitation spectroscopy on the 0.79-eV (c) line defect in irradiated silicon. *Phys. Rev. B* **29**, 7051–7053 (1984).
- Ishikawa, T., Koga, K., Itahashi, T., Itoh, K. M. & Vlasenko, L. S. Optical properties of triplet states of excitons bound to interstitial-carbon interstitial-oxygen defects in silicon. *Phys. Rev. B* **84**, 115204 (2011).
- Coutinho, J. et al. Interstitial carbon-oxygen center and hydrogen related shallow thermal donors in si. *Phys. Rev. B* **65**, 014109 (2001).
- Hayama, S. et al. Lattice isotope effects on optical transitions in silicon. *Phys. Rev. B* **70**, 035202 (2004).
- Ceperley, D. M. & Alder, B. J. Ground state of the electron gas by a stochastic method. *Phys. Rev. Lett.* **45**, 566–569 (1980).
- Perdew, J. P. & Zunger, A. Self-interaction correction to density-functional approximations for many-electron systems. *Phys. Rev. B* **23**, 5048–5079 (1981).
- Snyder, L., Wu, R. & Deak, P. The c' si' o' si' (c) four-member ring and the si-g15 centre. In *Early Stages of Oxygen Precipitation in Silicon*, 427–432 (Springer, 1996).
- Xiao, J. et al. Realistic dimension-independent approach for charged-defect calculations in semiconductors. *Phys. Rev. B* **101**, 165306 (2020).
- Hybertsen, M. S. & Louie, S. G. Electron correlation in semiconductors and insulators: band gaps and quasiparticle energies. *Phys. Rev. B* **34**, 5390–5413 (1986).
- Albrecht, S., Reining, L., Del Sole, R. & Onida, G. Ab initio calculation of excitonic effects in the optical spectra of semiconductors. *Phys. Rev. Lett.* **80**, 4510–4513 (1998).
- Rohlfing, M. & Louie, S. G. Electron-hole excitations in semiconductors and insulators. *Phys. Rev. Lett.* **81**, 2312–2315 (1998).
- Yin, C. et al. Optical addressing of an individual erbium ion in silicon. *Nature* **497**, 91–94 (2013).

42. Priolo, F., Franzò, G., Coffa, S. & Carnera, A. Excitation and nonradiative deexcitation processes of e^{-3+} in crystalline Si. *Phys. Rev. B* **57**, 4443–4455 (1998).
43. Weiss, L., Gritsch, A., Merkel, B. & Reiserer, A. Erbium dopants in nanophotonic silicon waveguides. *Optica* **8**, 40–41 (2021).
44. Gritsch, A., Weiss, L., Früh, J., Rinner, S. & Reiserer, A. Narrow optical transitions in erbium-implanted silicon waveguides. *Phys. Rev. X* **12**, 041009 (2022).
45. Ulanowski, A., Merkel, B. & Reiserer, A. Spectral multiplexing of telecom emitters with stable transition frequency. *Sci. Adv.* **8**, eabo4538 (2022).
46. Beaufils, C. et al. Optical properties of an ensemble of g-centers in silicon. *Phys. Rev. B* **97**, 035303 (2018).
47. Zhu, L., Yuan, S., Zeng, C. & Xia, J. Manipulating photoluminescence of carbon g-center in silicon metasurface with optical bound states in the continuum. *Adv. Opt. Mater.* **8**, 1901830 (2020).
48. Landau, L. D. Zur theorie der energieübertragung ii. *Phys. Z. Sowjetunion* **2**, 46–51 (1932).
49. Zener, C. & Fowler, R. H. Non-adiabatic crossing of energy levels. *Proc. R. Soc. A* **137**, 696–702 (1932).
50. Dutt, M. V. G. et al. Quantum register based on individual electronic and nuclear spin qubits in diamond. *Science* **316**, 1312–1316 (2007).
51. Robledo, L. et al. High-fidelity projective read-out of a solid-state spin quantum register. *Nature* **477**, 574–578 (2011).
52. Filidou, V. et al. Ultrafast entangling gates between nuclear spins using photoexcited triplet states. *Nat. Phys.* **8**, 596–600 (2012).
53. Bourassa, A. et al. Entanglement and control of single nuclear spins in isotopically engineered silicon carbide. *Nat. Mater.* **19**, 1319–1325 (2020).
54. Safonov, A. & Lightowers, E. Photoluminescence characterisation of hydrogen-related centres in silicon. *Mater. Sci. Eng. B* **58**, 39–47 (1999).
55. Hughes, M. A. et al. Spin echo from erbium implanted silicon. *Appl. Phys. Lett.* **118**, 194001 (2021).
56. Lee, S.-Y. et al. Readout and control of a single nuclear spin with a metastable electron spin ancilla. *Nat. Nanotechnol.* **8**, 487–492 (2013).
57. Foglszinger, J. et al. Tr12 centers in diamond as a room temperature atomic scale vector magnetometer. *NPJ Quantum Inf.* **8**, 65 (2022).
58. Krukau, A. V., Vydrov, O. A., Izmaylov, A. F. & Scuseria, G. E. Influence of the exchange screening parameter on the performance of screened hybrid functionals. *J. Chem. Phys.* **125**, 224106 (2006).
59. Kresse, G. & Hafner, J. Ab initio molecular dynamics for liquid metals. *Phys. Rev. B* **47**, 558–561 (1993).
60. Kresse, G. & Furthmüller, J. Efficient iterative schemes for ab initio total-energy calculations using a plane-wave basis set. *Phys. Rev. B* **54**, 11169–11186 (1996).
61. Kresse, G. & Furthmüller, J. Efficiency of ab-initio total energy calculations for metals and semiconductors using a plane-wave basis set. *Comput. Mater. Sci.* **6**, 15–50 (1996).
62. Paier, J. et al. Screened hybrid density functionals applied to solids. *J. Chem. Phys.* **124**, 154709 (2006).
63. Blöchl, P. E. Projector augmented-wave method. *Phys. Rev. B* **50**, 17953–17979 (1994).
64. Kresse, G. & Joubert, D. From ultrasoft pseudopotentials to the projector augmented-wave method. *Phys. Rev. B* **59**, 1758–1775 (1999).
65. Gali, A., Jánzén, E., Deák, P., Kresse, G. & Kaxiras, E. Theory of spin-conserving excitation of the $n - V^-$ center in diamond. *Phys. Rev. Lett.* **103**, 186404 (2009).
66. Chagas da Silva, M. et al. Self-consistent potential correction for charged periodic systems. *Phys. Rev. Lett.* **126**, 076401 (2021).
67. Bodrog, Z. & Gali, A. The spin–spin zero-field splitting tensor in the projector-augmented-wave method. *J. Phys. Condens. Matter* **26**, 015305 (2013).
68. Perdew, J. P., Burke, K. & Ernzerhof, M. Generalized gradient approximation made simple. *Phys. Rev. Lett.* **77**, 3865–3868 (1996).
69. Sander, T., Maggio, E. & Kresse, G. Beyond the tamm-dancoff approximation for extended systems using exact diagonalization. *Phys. Rev. B* **92**, 045209 (2015).
70. Baryshnikov, G., Minaev, B. & Ågren, H. Theory and calculation of the phosphorescence phenomenon. *Chem. Rev.* **117**, 6500–6537 (2017).

ACKNOWLEDGEMENTS

A.G. acknowledges the Hungarian NKFIH grant No. KKP129866 of the National Excellence Programme of Quantum-coherent materials project and the EU H2020 project QuanTELCO (Grant No. 862721). This research was supported by the Ministry of Culture and Innovation and the National Research, Development and Innovation Office within the Quantum Information National Laboratory of Hungary (Grant No. 2022-2.1.1-NL-2022-00004). We acknowledge KIFÜ for awarding us access to high-performance computation resource based in Hungary. Open access funding provided by ELKH Wigner Research Centre for Physics.

AUTHOR CONTRIBUTIONS

P.U. and P.D. carried out the DFT calculations under the supervision of A.G. P.U. and A.P. analysed the results and conceived the quantum optics protocols under the supervision of A.G. All authors contributed to the discussion and writing of the paper. A.G. conceived and led the entire scientific project.

COMPETING INTERESTS

The authors declare no competing interests.

ADDITIONAL INFORMATION

Supplementary information The online version contains supplementary material available at <https://doi.org/10.1038/s41524-022-00957-7>.

Correspondence and requests for materials should be addressed to Adam Gali.

Reprints and permission information is available at <http://www.nature.com/reprints>

Publisher's note Springer Nature remains neutral with regard to jurisdictional claims in published maps and institutional affiliations.



Open Access This article is licensed under a Creative Commons Attribution 4.0 International License, which permits use, sharing, adaptation, distribution and reproduction in any medium or format, as long as you give appropriate credit to the original author(s) and the source, provide a link to the Creative Commons license, and indicate if changes were made. The images or other third party material in this article are included in the article's Creative Commons license, unless indicated otherwise in a credit line to the material. If material is not included in the article's Creative Commons license and your intended use is not permitted by statutory regulation or exceeds the permitted use, you will need to obtain permission directly from the copyright holder. To view a copy of this license, visit <http://creativecommons.org/licenses/by/4.0/>.

© The Author(s) 2022